Journal of Organometallic Chemistry 713 (2012) 112–122

Contents lists available at SciVerse ScienceDirect

Journal of Organometallic Chemistry

journal homepage: www.elsevier.com/locate/jorganchem

Synthesis and structural characterization of new piano-stool ruthenium(II) complexes bearing 1-butylimidazole heteroaromatic ligand

Tânia S. Morais [a], M. Helena Garcia [a,e,*], M. Paula Robalo [b,c], M.F.M. Piedade [c,e], M. Teresa Duarte [c], M. José Villa de Brito [c,e], Paulo J. Amorim Madeira [d]

[a] Centro de Ciências Moleculares e Materiais, Faculdade de Ciências da Universidade de Lisboa, Campo Grande, 1749-016 Lisboa, Portugal
[b] Departamento de Engenharia Química, Instituto Superior de Engenharia de Lisboa, Av. Conselheiro Emídio Navarro, 1, 1959-007 Lisboa, Portugal
[c] Centro de Química Estrutural, Complexo I, Instituto Superior Técnico, Av. Rovisco Pais, 1049-001 Lisboa, Portugal
[d] Centro de Química e Bioquímica, Faculdade de Ciências da Universidade de Lisboa, Campo Grande, 1749-016 Lisboa, Portugal
[e] Departamento de Química e Bioquímica, Faculdade de Ciências da Universidade de Lisboa, Campo Grande, 1749-016 Lisboa, Portugal

ARTICLE INFO

Article history:
Received 15 March 2012
Received in revised form
20 April 2012
Accepted 24 April 2012

Keywords:
Ruthenium(II)
Cyclic voltametry
X-ray crystal structures
Monocyclopentadienyl complexes
1-Butylimidazole

ABSTRACT

New cationic ruthenium(II) complexes with the formula [Ru(η^5-C_5H_5)(LL)(1-BuIm)] [Z], with (LL) = 2PPh_3 or DPPE, and $Z = CF_3SO_3^-$, PF_6^-, BPh_4^-, have been synthesized and fully characterized. Spectroscopic and electrochemical studies revealed that the electronic properties of the coordinated 1-butylimidazole were clearly influenced by the nature of the phosphane coligands (LL) and also by the different counter ions. The solid state structures of the six complexes determined by X-ray crystallographic studies, confirmed the expected distorted three-legged piano stool structure. However the geometry of the 1-butylimidazole ligand was found considerably different in all six compounds, being governed by the stereochemistry of the mono and bidentate coligands (PPh_3 or DPPE).

1. Introduction

Ruthenium coordination compounds have attracted much attention as antitumor agents, since these compounds revealed already properties that can be an advantage to antitumor platinum(II) complexes currently used in clinic [1–4]. One of the most significant features is the reduced toxicity of ruthenium compounds, which is in part due to the ability of ruthenium to mimic the iron in binding to biological molecules. Besides, the non-cross-resistance and a novel mechanism of action [5,6] in cisplatin-resistant cancer cells together with the prospect of a different spectrum of activity [7,8], make the study of ruthenium complexes a particular attractive area for the search of new drugs. However coordination compounds present some problems concerning clinical trials related to their instability and complicated ligand exchange chemistry. To overcome this situation the organometallic chemistry appeared as an attractive area of research to provide organo-ruthenium complexes as suitable drug candidates. The families of ruthenium(II) organometallic compounds studied, so far, for this purpose present a half sandwich structure mainly based on η^6-arene substituted ligands. Many results are reported in the literature revealing potent cytotoxicity, against a range of tumor cell lines, for two families of these Ru(II) derivatives [9,10].

Our approach in this field lead us to the synthesis and study of half sandwich cationic compounds derived of "Ru(η^5-C_5H_5)" fragment, containing N-heteroaromatic sigma coordinated ligands. The new studied compounds revealed significant effect of toxicity in Lovo and MiaPaCa cells [11], human leukemia cancer cells (HL-60) with IC_{50} values lower than that of cisplatin [12,13].

Our promising results obtained for compounds with imidazole [11], which cytotoxicity is in the nanomolar range, encouraged us to continue these studies and synthesize a set of new compounds bearing an imidazole derivative molecule. The chosen molecule was 1-butylimidazole, which flexible side chain can impart ability to the molecule for different type of interactions. Moreover, in order to play with the electronic properties of the organometallic fragment and consequently, the electronic density on the ring of 1-butylimidazole, two different phosphanes were used as coligands, PPh_3 and DPPE. Finally, changes in the counter ion were also

* Corresponding author. Faculdade de Ciências da Universidade de Lisboa, EdifícioC8, Campo Grande, 1749-016 Lisboa, Portugal. Tel.: +351 217500972; fax: +351 217500088.
E-mail address: lena.garcia@fc.ul.pt (M.H. Garcia).

0022-328X/$ – see front matter © 2012 Elsevier B.V. All rights reserved.
doi:10.1016/j.jorganchem.2012.04.024

considered, having in mind studies reporting considerable changes in the biological activity of the compounds. In fact, different counter ions are expected to lead to diverse ion-pair formation which can account for a number of physiochemical phenomena involving the wide-ranging lipophilic parts of the molecule [14–22].

The structures of the six new compounds [23], here presented, were determined by X-ray diffraction studies. Spectroscopic and electrochemical data obtained by cyclic voltammetry were analyzed in order to get some understanding about the electronic π-coupling between the η^5-cyclopentadienylruthenium fragment and the π-system of the imidazole ring. The overall results are analyzed in perspective of further studies of interaction of these compounds with DNA.

2. Experimental

2.1. General procedures

All the experiments were carried out under dinitrogen atmosphere using current Schlenk techniques and solvents used were dried using standard methods [24]. Starting materials [Ru(η^5-C_5H_5)(LL)Cl] were prepared following the methods described in the literature: LL = $2PPh_3$ [25] and DPPE [26]. ^{1}H- ^{13}C and ^{31}P NMR spectra were recorded on a Bruker Avance 400 spectrometer at probe temperature. ^{1}H and ^{13}C chemical shifts (s = singlet; d = duplet; t = triplet; quint = quintet; sep = septet; m = multiplet for ^{1}H) are reported in parts per million (ppm) downfield from internal Me_4Si and ^{31}P NMR spectra are reported in ppm downfield from external standard H_3PO_4 85%. FT-IR spectra were recorded in a Mattson Satellite FT-IR spectrophotometer with KBr; only significant bands are cited in the text w = weak; vw = very weak; m = medium; s = sharp; vs = very sharp. ESI-HRMS spectra were acquired in an Apex Ultra FTICR Mass Spectrometer equipped with an Apollo II Dual ESI/MALDI ion source, from Bruker Daltonics, and a 7T actively shielded magnet fromMagnex Scientific. Electronic spectra were recorded at room temperature on UV-1603 Shimadzu UV–visible spectrometer in the range of 200–900 nm.

2.2. Synthesis of the Ru(II) complexes

2.2.1. [Ru(η^5-C_5H_5)(PPh_3)$_2$(1-BuIm)][CF_3SO_3] **1**

To a stirred solution of [Ru(η^5-C_5H_5)(PPh_3)$_2$Cl] (0.32 g, 0.5 mmol) in dichloromethane (25 mL) was added 1-butylimidazole (0.06 mL, 0.6 mmol) and $AgCF_3SO_3$ (0.15, 0.6 mmol). After refluxing for 5 h the solution turned from orange to yellow. The reaction mixture was cooled to room temperature, filtered and the solvent removed under reduced pressure; the product was washed with n-hexane (2 × 10 mL) affording yellow crystals after recrystallization from dichloromethane/diethyl ether. Yield: 77%. ^{1}H NMR [$CDCl_3$, Me_4Si, δ/ppm]: 7.62 [s, 1, H1], 7.37 [m, 6, H_{para}(PPh_3)], 7.22 [m, 12, H_{meta} (PPh_3)], 7.01 [m, 12, H_{ortho}(PPh_3)], 6.63 [t, 1, H3, $^3J_{HH}$ = 1.72 Hz], 6.59 [t, 1, H_2, $^3J_{HH}$ = 1.72 Hz], 4.41 [s, 5, η^5-C_5H_5], 3.79 [t, 2, H4, $^3J_{HH}$ = 7.01 Hz], 1.43 [quintet, 2, H5, $^3J_{HH}$ = 7.03 Hz], 0.97 [sextet, 2, H6, $^3J_{HH}$ = 7.94 Hz], 0.77 [t, 3, H7, $^3J_{HH}$ = 7.03 Hz]. ^{13}C NMR [$CDCl_3$, δ/ppm]: 143.64 (C_1, 1-BuIm), 136.64 (Cq, PPh_3), 135.65 (CH, PPh_3), 130.01 (CH, PPh_3), 128.06 (CH, PPh_3), 135.35 (C_2, 1-BuIm), 120.14 (C_3, 1-BuIm), 82.77 (C_5H_5), 47.64 (C_4, 1-BuIm), 32.57 (C_5, 1-BuIm), 19.26 (C_6, 1-BuIm), 13.61 (C_7, 1-BuIm). ^{31}P NMR [$CDCl_3$, δ/ppm]: 42.48 [s, PPh_3]. IV [KBr, cm^{-1}]: 3433 (m), 3124 (m), 3051 (m), 2960 (m), 2931 (w), 2873 (w), 1969 (vw), 1907 (vw), 1828 (vw), 1637 (vw), 1529 (vw), 1479 (m), 1435 (s), 1344 (vw), 1279 (vs), 1255 (vs), 1223 (m), 1159 (s), 1088 (s), 1030 (vs), 997 (w), 924 (vw), 887 (vw), 843 (w), 816 (w), 742 (s), 696 (vs), 636 (s), 571 (vw), 517 (vs), 420 (w). ESI-HRMS: calcd. For [M$^+$] 815.22653, found 815.22393.

2.2.2. [Ru(η^5-C_5H_5)(PPh_3)$_2$(1-BuIm)][PF_6] **2**

To a solution of [Ru(η^5-C_5H_5)(PPh_3)$_2$Cl] (0.32 g, 0.5 mmol) in dichloromethane (25 mL) was added 1-butylimidazole (0.06 mL, 0.6 mmol) followed by the addition of $TlPF_6$ (0.21, 0.6 mmol). The reaction is carried out at room temperature with vigorous stirring during 2 h with the change of color orange to brown. The precipitate of TlCl was removed by cannula-filtration and the solvent evaporated. The product was washed with n-hexane (2 × 10 mL) affording brown crystals after recrystallization from dichloromethane/n-hexane. Yield: 43%. ^{1}H NMR [$(CD_3)_2CO$, Me_4Si, δ/ppm]: 7.48 [m, 6, H_{para}(PPh_3)], 7.34 [m, 12, H_{meta}(PPh_3)], 7.20 [s, 1, H1], 7.13 [m, 14, H_{ortho}(PPh_3) + H3 + H2], 4.56 [s, 5, η^5-C_5H_5], 3.31 [t, 2, H4, $^3J_{HH}$ = 6.63 Hz], 1.43 [quintet, 2, H5, $^3J_{HH}$ = 7.16 Hz], 0.94 [sextet, 2, H6, $^3J_{HH}$ = 7.96 Hz], 0.76 [t, 3, H7, $^3J_{HH}$ = 7.27 Hz]. ^{13}C NMR [$(CD_3)_2CO$, δ/ppm]: 143.83 (C_1, 1-BuIm), 137.52 (Cq, PPh_3), 134.43 (CH, PPh_3), 130.90 (CH, PPh_3), 129.21 (CH, PPh_3), 136.60 (C_2, 1-BuIm), 121.55 (C_3, 1-BuIm), 83.41 (C_5H_5), 48.17 (C_4, 1-BuIm), 33.04 (C_5, 1-BuIm), 19.81 (C_6, 1-BuIm), 13.70 (C_7, 1-BuIm). ^{31}P NMR [$(CD_3)_2CO$, δ/ppm]: 42.23 [s, PPh_3], −144.12 [septet, PF_6]. IV [KBr, cm^{-1}]: 3435 (m), 3143 (m), 3051 (m), 2959 (m), 2928 (m), 2856 (w), 1518 (w), 1480 (m), 1420 (s), 1419 (w), 1312 (vw), 1262 (w), 1233 (vw), 1184 (w), 1159 (vw), 1119 (m), 1086 (s), 1027 (w), 998 (vw), 910 (vw), 839 (vs), 748 (s), 695 (vs), 668 (m), 618 (vw), 587 (w), 557 (m), 520 (s), 463 (w), 419 (w). ESI-HRMS: calcd. For [M$^+$] 815.22653, found 815.22565.

2.2.3. [Ru(η^5-C_5H_5)(PPh_3)$_2$(1-BuIm)][BPh_4] **3**

To a suspension of [Ru(η^5-C_5H_5)(PPh_3)$_2$Cl] (0.32 g, 0.5 mmol) in methanol (25 mL) was added 1-butylimidazole (0.06 mL, 0.6 mmol) followed by the addition of NH_4BPh_4 (0.20, 0.6 mmol). After 3 h and 30 min the yellow powder which separated was filtered, washed with n-hexane (2 × 10 mL), and vacuum dried, affording yellow crystals after recrystallization from dichloromethane/n-hexane. Yield: 87%. ^{1}H NMR [$(CD_3)_2CO$, Me_4Si, δ/ppm]: 7.47 [m, 6, H_{para} (PPh_3)], 7.33 [m, 20, H_{meta}(PPh_3) + H_{ortho}(BPh_4)], 7.22 [t, 1, H3, $^3J_{HH}$ = 1.46 Hz], 7.13 [m, 13, H1 + H_{ortho}(PPh_3)], 7.07 [t, 1, H2, $^3J_{HH}$ = 1.48 Hz], 6.92 [m, 8, H_{para}(BPh_4)], 6.77 [m, 4, H_{para}(BPh_4)], 4.55 [s, 5, η^5-C_5H_5], 3.67 [t, 2, H4, $^3J_{HH}$ = 6.96 Hz], 1.42 [quint, 2, H5, $^3J_{HH}$ = 6.23 Hz], 0.93 [sextet, 2, H6, $^3J_{HH}$ = 7.45 Hz], 0.76 [t, 3, H7, $^3J_{HH}$ = 7.25 Hz]. ^{13}C NMR [$(CD_3)_2CO$, δ/ppm]: 143.75 (C_1, 1-BuIm), 137.48 (Cq, PPh_3), 137.29 (Cq, BPh_4), 137.03 (CH, BPh_4), 136.61 (C_2, 1-BuIm), 134.41 (CH, PPh_3), 130.90(CH, PPh_3), 129.21 (CH, PPh_3), 125.95 (CH, BPh_4), 122.21 (CH, BPh_4), 121.56 (C_3, 1-BuIm), 83.38 (C_5H_5), 48.21 (C_4, 1-BuIm), 33.09 (C_5, 1-BuIm), 19.82 (C_6, 1-BuIm), 13.75 (C_7, 1-BuIm). ^{31}P NMR [$(CD_3)_2CO$, δ/ppm]: 42.23 [s, PPh_3]. IV [KBr, cm^{-1}]: 3416 (w), 3140 (w), 3124 (m), 3051 (s), 2997 (m), 2983 (m), 2955 (m), 2929 (m), 2862 (w), 1946 (vw), 1890 (vw), 1818 (vw), 1589 (m), 1531 (m), 1479 (s), 1431 (s), 1310 (w), 1237 (w), 1104 (w), 1089 (s), 1029 (w), 998 (w), 826 (w), 734 (s), 689 (vs), 612 (m), 535 (s), 522 (vs), 494 (s), 468 (m), 421 (m). ESI-HRMS: calcd. For [M$^+$] 815.22653, found 815.22964.

2.2.4. [Ru(η^5-C_5H_5)(DPPE)(1-BuIm)][CF_3SO_3] **4**

To a stirred solution of [Ru(η^5-C_5H_5)(DPPE)Cl] (0.30 g, 0.5 mmol) in dichloromethane (25 mL) was added 1-butylimidazole (0.06 mL, 0.6 mmol) and $AgCF_3SO_3$ (0.15, 0.6 mmol). After refluxing for 10 h the solution turned from orange to yellow. The reaction mixture was cooled to room temperature, filtered and the solvent removed under reduced pressure; the product was washed with n-hexane (2 × 10 mL) affording yellow crystals after recrystallization from dichloromethane/n-hexane. Yield: 83%. ^{1}H NMR [$(CD_3)_2CO$, Me_4Si, δ/ppm]: 7.70 [t, 4, DPPE], 7.41 [m, 4, DPPE], 6.62 [t, 1, H 3, $^3J_{HH}$ = 1.37 Hz], 6.57 [s, 1, H1], 6.34 [t, 1, H2, $^3J_{HH}$ = 1.35 Hz], 4.75 [s, 5, η^5-C_5H_5], 3.40 [t, 2, H4, $^3J_{HH}$ = 7.35 Hz], 2.96 [m, 4, CH2 (DPPE)], 1.19 [quint, 2, H5, $^3J_{HH}$ = 7.27 Hz], 0.91 [sextet, 2, H6, $^3J_{HH}$ = 7.64 Hz], 0.76 [t, 3, H7, $^3J_{HH}$ = 7.30 Hz]. ^{13}C NMR [$(CD_3)_2CO$, δ/ppm]: 143.65

[C_1, 1-BuIm], 135.30 [C_2, 1-BuIm], 133.86 [CH, DPPE], 131.63 [CH, DPPE], 131.07 [Cq, DPPE], 129.42 [CH, DPPE], 120.20 [C_3, 1-BuIm], 82.96 [C_5H_5], 47.61 [C_4, 1-BuIm], 33.17 [C_5, 1-BuIm], 29.12 [CH2, DPPE], 19.96 [C_6, 1-BuIm], 13.70 [C_7, 1-BuIm]. ^{31}P NMR [$(CD_3)_2CO$, δ/ppm]: 83.35 [s, DPPE]. IV [KBr, cm^{-1}]: 3415 (w), 3136 (m), 3053 (w), 2950 (m), 2933 (m), 2867 (w), 1968 (vw), 1896 (vw), 1825 (vw), 1571 (w), 1530 (w), 1478 (w), 1435 (m), 1372 (vw), 1352 (vw), 1268 (vs), 1224 (m), 1186 (w), 1149 (s), 1093 (m), 1030 (vs), 994 (w), 916 (vw), 875 (w), 807 (m), 752 (m), 689 (s), 637 (vs), 674 (m), 531 (s), 517 (s), 497 (m), 440 (m). ESI-HRMS: calcd. For [M^+] 689.17932, found 689.17777.

2.2.5. [Ru(η^5-C_5H_5)(DPPE)(1-BuIm)][PF_6] **5**

To a solution of [Ru(η^5-C_5H_5)(DPPE)Cl] (0.30 g, 0.5 mmol) in dichloromethane (25 mL) was added 1-butylimidazole (0.06 mL, 0.6 mmol) followed by the addition of TlF_6 (0.21, 0.6 mmol). After refluxing for 5 h the solution turned from orange to yellow. The reaction mixture was cooled to room temperature, filtered and the solvent removed under reduced pressure; the product was washed with n-hexane (2 × 10 mL) affording yellow crystals after recrystallization from dichloromethane/n-hexane. Yield: 78%. ^{1}H NMR [$(CD_3)_2CO$, Me_4Si, δ/ppm]: 7.69 [t, 4, DPPE], 7.39 [m, 4, DPPE], 6.63 [t, 1, H $_3$, $^3J_{HH}$ = 1.49 Hz], 6.53 [s, 1, H1], 6.36 [t, 1, H2, $^3J_{HH}$ = 1.48 Hz], 4.75 [s, 5, η^5-C_5H_5], 3.39 [t, 2, H4, $^3J_{HH}$ = 7.33 Hz], 2.96 [m, 4, CH_2 (DPPE)], 1.19 [quint, 2, H5, $^3J_{HH}$ = 7.34 Hz], 0.90 [sextet, 2, H6, $^3J_{HH}$ = 7.64 Hz], 0.76 [t, 3, H7, $^3J_{HH}$ = 7.11 Hz]. ^{13}C NMR [$(CD_3)_2CO$, δ/ppm]: 143.62 [C_1, 1-BuIm], 135.35 [C_2, 1-BuIm], 133.85 [CH, DPPE], 131.63 [CH, DPPE], 131.09 [Cq, DPPE], 129.46 [CH, DPPE], 120.30 [C_3, 1-BuIm], 82.88 [C_5H_5], 47.62 [C_4, 1-BuIm], 33.15 [C_5, 1-BuIm], 29.15 [CH_2, DPPE], 20.07 [C_6, 1-BuIm], 13.69 [C_7, 1-BuIm]. ^{31}P NMR [$(CD_3)_2CO$, δ/ppm]: 83.37 [s, DPPE], −144.24 [septet, PF_6]. IV [KBr, cm^{-1}]: 3426 (w), 3151 (m), 3058 (w), 2959 (m), 2922 (m), 2862 (w), 1965 (vw), 1890 (vw), 1814 (vw), 1654 (vw), 1521 (m), 1479 (m), 1435 (s), 1416 (m), 1307 (vw), 1240 (m), 1181 (w), 1096 (s), 1028 (w), 999 (m), 918 (w), 837 (vs), 752 (m), 733 (m), 697 (s), 675 (m), 645 (w), 587 (vw), 557 (s), 529 (s), 517 (m), 497 (m), 438 (m). ESI-HRMS: calcd. For [M^+] 689.17932, found 689.17982.

2.2.6. [Ru(η^5-C_5H_5)(DPPE)(1-BuIm)][BPh_4] **6**

To a solution of [Ru(η^5-C_5H_5)(DPPE)Cl] (0.30 g, 0.5 mmol) in methanol (25 mL) was added 1-butylimidazole (0.06 mL, 0.6 mmol) followed by the addition of NH_4BPh_4 (0.20, 0.6 mmol).

After refluxing for 4 h the solution was filtered and the solvent removed under reduced pressure. The yellow powder was dissolved in acetone and the precipitate of NH_4Cl was removed by cannula-filtration and the solvent evaporated. The product was washed with n-hexane (2 × 10 mL) affording yellow crystals after recrystallization from dichloromethane/n-hexane. Yield: 81%. ^{1}H NMR [$(CD_3)_2CO$, Me_4Si, δ/ppm]: 7.68 [t, 4, DPPE] 7.38 [m, 24, DPPE + $H_{ortho}(BPh_4)$], 6.60 [t, 1, H3, $^3J_{HH}$ = 1.37 Hz], 6.50 [s, 1, H1], 6.35 [t, 1, H2, $^3J_{HH}$ = 1.34 Hz], 6.92 [m, 8, H_{para} (BPh_4)], 6.77 [m, 4, H_{para} (BPh_4)], 4.74 [s, 5, η^5-C_5H_5], 3.37 [t, 2, H4, $^3J_{HH}$ = 7.17 Hz], 2.93 [m, 4, CH_2 (DPPE)], 1.18 [quint, 2, H5, $^3J_{HH}$ = 6.96 Hz], 0.89 [sextet, 2, H6, $^3J_{HH}$ = 7.60 Hz], 0.76 [t, 3, H7, $^3J_{HH}$ = 7.29 Hz]. ^{13}C NMR [$(CD_3)_2CO$, δ/ppm]: 143.51 [C_1, 1-BuIm], 135.37 [C_2, 1-BuIm], 137.03 (CH, BPh_4), 133.84 [CH, DPPE], 131.63 [CH, DPPE], 131.10 [Cq, DPPE], 130.56 (Cq, BPh_4), 129.36 [CH, DPPE], 125.95 (CH, BPh_4), 122.21 (CH, BPh_4), 120.23 [C_3, 1-BuIm], 82.73 [C_5H_5], 47.63 [C_4, 1-BuIm], 33.14 [C_5, 1-BuIm], 29.11 [CH_2, DPPE], 19.97[C_6, 1-BuIm], 13.70 [C_7, 1-BuIm]. ^{31}P NMR [$(CD_3)_2CO$, δ/ppm]: 83.46 [s, DPPE]. IV [KBr, cm^{-1}]: 3433 (w), 3125 (m), 3053 (m), 3038 (m), 2998 (w), 2932 (w), 2873 (vw), 1946 (vw), 1886 (vw), 1804 (vw), 1578 (m), 1529 (w), 1481 (m), 1434 (s), 1408 (m), 1236 (w), 1184 (vw), 1091 (s), 1030 (w), 1000 (w), 989 (w), 868 (w), 840 (w), 799 (m), 746 (s), 732 (s), 699 (vs), 672 (s), 641 (m), 611 (s), 530 (s), 520 (s), 496 (m), 469 (w), 441 (w). ESI-HRMS: calcd. For [M^+] 689.17932, found 689.17980.

2.3. Electrochemical studies

Cyclic voltammograms were obtained using a EG&G Princeton Applied Research Potentiostat/Galvanostat Model 273A equipped with Electrochemical PowerSuite v2.51 software for electrochemical analysis, in anhydrous dichloromethane or acetonitrile with tetrabutylammonium hexafluorophosphate (0.1–0.2 M) as supporting electrolyte. The electrochemical cell was a homemade three electrode configuration cell with a platinum-disc working electrode (1.0 mm) probed by a Luggin capillary connected to a silver-wire pseudo-reference electrode and a platinum wire auxiliary electrode. All the experiments were performed in nitrogen atmosphere at room temperature. All the potentials reported were measured against the ferrocene/ferrocenium redox couple as internal standard and normally quoted relative to SCE (using the ferrocenium/ferrocene redox couple $E_{1/2}$ = 0.46 or 0.40 V versus SCE for dichloromethane or acetonitrile respectively [27]).

Both the sample and the electrolyte (Fluka) were dried under vacuum for several hours prior to the experiment. Reagent grade solvents were dried, purified by standard procedures and distilled under nitrogen atmosphere before use.

2.4. Crystal structure determination

X-ray data were collected on a Brucker AXS APEX CCD are detector diffracometer at 150(1) K using graphite-monochromated Mo Kα (λ = 0.71073 Å) radiation. Intensity data were corrected for Lorentz polarization effects. Empirical absorption correction using SADABS [28] was applied and data reduction was done with SMART and SAINT programs [29].

The structures were solved by direct methods with the programs SIR97 [30] and SHELXS97 [31] and refined by full-matrix least squares on F^2 with SHELXL97 [32] both included in the package of programs WINGX-Version 1.70.01 [33]. Non-hydrogen atoms were refined with anisotropic thermal parameters whereas H-atoms placed in idealized positions and allowed to refine riding on the parent C atom. Graphical representations were prepared using ORTEP [34] and Mercury 1.1.2 [35].

A summary of the crystal data, structure solution and refinement parameters for all structures are givens in Tables 1 and 2.

3. Results and discussion

3.1. Synthesis of the Ru(II) complexes

The novel cationic complexes of general formula [Ru(η^5-C_5H_5)(LL)(1-BuIm)][Z], with (LL) = 2PPh_3 or DPPE, and $Z = CF_3SO_3^-$, PF_6^-, BPh_4^-, were prepared by halide abstraction with $AgCF_3SO_3$, $TlPF_6$ or NH_4BPh_4, from the neutral complexes [Ru(η^5-C_5H_5)(LL)Cl], in dichloromethane or methanol, in the presence of a slight excess of the 1-butylimidazole ligand (Scheme 1). The reactions were carried out at reflux or stirring at room temperature. The compounds were recrystallized by slow diffusion of diethyl ether or n-hexane in dichloromethane solutions. The new compounds were fully characterized by FT-IR, ^{1}H, ^{13}C, and ^{31}P NMR spectroscopies. The solid state FT-IR spectra of the complexes present the characteristic band of the cyclopentadienyl ligand in the range 3051–3058 cm^{-1}, the PF_6^- (840 and 560 cm^{-1}), $CF_3SO_3^-$ anion (1250 cm^{-1}) or BPh_4^- anion (730–745 cm^{-1}) and the imidazole ring (CH stretch) in the range 3124–3151 cm^{-1} All the new compounds were also characterized by X-ray diffraction studies.

Table 1
Data collection and structure refinement parameters for [Ru(η^5-C_5H_5)(PPh_3)$_2$(1-BuIm)][CF_3SO_3] 1, [Ru(η^5-C_5H_5)(PPh_3)$_2$(1-BuIm)][PF_6] 2, [Ru(η^5-C_5H_5)(PPh_3)$_2$(1-BuIm)][BPh_4] 3.

Compound	**1**	**2**	**3**
Empirical formula	$C_{49.50}H_{48}ClF_3N_2O_3P_2RuS$	$C_{49}H_{49}Cl_2F_6N_2P_3Ru$	$C_{72}H_{67}BN_2P_2Ru$
Formula weight	1006.42	1044.78	1134.10
T (K)	150(2)	150(2)	296(2)
Wavelength (Å)	0.71073	0.71069	0.71073
Crystal system	Monoclinic	Triclinic	Orthorhombic
Space group	$P2_1/c$	P-1	P c a 2_1
Unit cell dimensions			
a (Å)	14.3039(16)	10.7473(4)	23.5845(5)
b (Å)	43.934(4)	11.3403(4)	18.5011(5)
c (Å)	14.6701(17)	21.2344(8)	26.0889(7)
α (°)	90	78.882(2)	90
B (°)	97.339(5)	79.672(2)	90
Γ (°)	90	71.227(2)	90
Volume (Å^3)	9143.5(17)	2385.12(15)	11,383.6(5)
Z	8	2	8
Calculated density (Mgm^{-3})	1.462	1.455	1.323
Absorption Coefficient (mm^{-1})	0.574	0.601	0.378
F (000)	4136	1068	4736
θ Range for data collection (°)	1.44–27.52	2.99–26.78	1.10–27.52
Limiting indices	$-18 \le h \le 17$ $-57 \le k \le 55$ $-16 \le l \le 19$	$-13 \le h \le 13$, $-14 \le k \le 11$, $-26 \le l \le 26$	$-30 \le h \le 18$, $-24 \le k \le 23$, $-33 \le l \le 33$
Reflections collected/unique	74,424/20,934 [*R*(int) = 0.1890]	36,624/10,064 [*R*(int) = 0.0680]	63,147/25,594 [*R*(int) = 0.0438]
Completeness to Refinement method	θ = 27.52 [99.5%]	θ = 26.78 [98.7%]	θ = 27.52 [99.7%]
Refinement method	Full-matrix least-squares on F^2 20,934/0/1126	Full-matrix least-squares on F^2 10,064/6/571	Full-matrix least-squares on F^2 15,594/1/1405
Goodness-on-fit on F^2	0.874	1.006	1.047
Final *R* indices [I > 2σ(I)]	R_1 = 0.0716 wR_2 = 0.1448	R_1 = 0.0451 wR_2 = 0.0820	R_1 = 0.0375 wR_2 = 0.0875
R indices (all data)	R_1 = 0.2054 wR_2 = 0.2068	R_1 = 0.0781 wR_2 = 0.0926	R_1 = 0.0554 wR_2 = 0.1113
Largest diff. peak and hole (eÅ)$^{-3}$	1.012 and −0.965	0.689 and −0.723	0.659 and −0.663

Table 2
Data collection and structure refinement parameters for [Ru(η^5-C_5H_5)(DPPE)(1-BuIm)][CF_3SO_3] 4, [Ru(η^5-C_5H_5)(DPPE)(1-BuIm)][PF_6] 5, [Ru(η^5-C_5H_5)(DPPE)(1-BuIm)][BPh_4] 6.

Compound	**4**	**5**	**6**
Empirical formula	$C_{39}H_{41}F_3N_2O_3P_2RuS$	$C_{38}H_{41}F_6N_2P_3Ru$	$C_{62}H_{57}BN_2P_2Ru$
Formula weight	837.81	833.71	1003.92
T (K)	150(2)	150(2)	150(2)
Wavelength (Å)	0.71073	0.71073	0.71073
Crystal system	Monoclinic	Monoclinic	Monoclinic
Space group	$P2_1/n$	$P2_1/n$	$P2_1/n$
Unit cell dimensions			
a (Å)	14.2788 (10)	13.6741(10)	9.925
b (Å)	16.4575(11)	16.5051(12)	21.064
c (Å)	16.6624(12)	16.8448(12)	24.132
α (°)	90	90	90
β (°)	107.585(2)	106.711(4)	95.17
γ (°)	90	90	90
Volume (Å^3)	3732.6(5)	3641.2(5)	5024.5
Z	4	4	4
Calculated density (Mgm^{-3})	1.491	1.521	1.327
Absorption coefficient (mm^{-1})	0.617	0.624	0.418
F (000)	1720	1704	2088
θ Range for data collection (°)	2.83–27.99	2.58–25.02	2.49–28.37
Limiting indices	$-18 \le h \le 16$, $-21 \le k \le 20$, $-21 \le l \le 20$	$-16 \le h \le 16$, $-19 \le k \le 19$, $-20 \le l \le 20$	$-13 \le h \le 13$ $-28 \le k \le 28$ $-32 \le l \le 32$
Reflections collected/unique	34,811/8925 [*R*(int) = 0.0952]	83,462/6378 [*R*(int) = 0.0520]	48,511/12,473 [*R*(int) = 0.0748]
Completeness to refinement method	θ = 27.99 [99.1%]	θ = 25.02 [99.2%]	θ = 28.37 [99.2%]
Refinement method	Full-matrix least-squares on F^2	Full-matrix least-squares on F^2	Full-matrix least-squares on F^2
Data/restraints/parameters	8925/0/460	6378/1/451	12,473/0/613
Goodness-on-fit on F^2	0.952	1.042	0.998
Final *R* indices [I > 2σ(I)]	R_1 = 0.0384 wR_2 = 0.0753	R_1 = 0.0441 wR_2 = 0.1111	R_1 = 0.0488 wR_2 = 0.1106
R indices (all data)	R_1 = 0.0671 wR_2 = 0.0840	R_1 = 0.0553 wR_2 = 0.1175	R_1 = 0.0845 wR_2 = 0.1275
Largest diff. peak and hole (eÅ)$^{-3}$	1.062 and −0.682	2.136 to −0.790	1.279 and −0.750

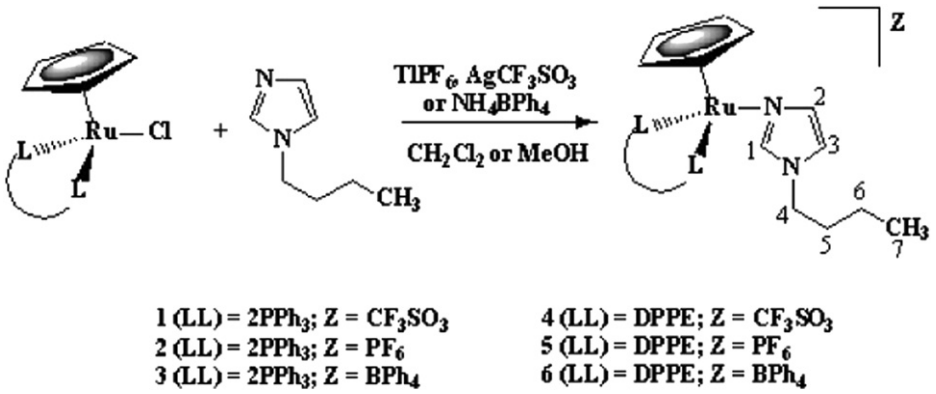

Scheme 1. Reaction scheme for the synthesis of Ru (II) complexes [Ru(η^5-C_5H_5)(LL)(1-BuIm)][Z] with numbering scheme for NMR purposes.

3.2. Spectroscopic studies by NMR

^{1}H NMR resonances of the cyclopentadienyl ring are in the characteristic range of monocationic ruthenium(II). The coordinated 1-BuIm ligand displays a general shielding of the protons as result of π backdonation from de organometallic moiety, with special relevance for H1, which up field shift was about 1 ppm for compounds **4**, **5** and **6** (see Scheme 1 for protons identification). Compounds with PPh_3 (**1**, **2** and **3**) showed only an up field shift of ~0.4 ppm on that proton H1, being these results in good agreement with the better donor character of DPPE. Moreover, the remaining protons of the coordinated heteroaromatic ring, H2 and H3, display a slight deshielding (~0.3 ppm) revealing that the income of π electronic density did not compensate the effect of sigma coordination on this side of the ring, which is the longest way between the two N atoms. Furthermore, also an increased electronic density was found at the coordinated 1-butylimidazole pendent arm. In fact, protons H4 and H5 are shielded up to 0.6 and 0.5 ppm relatively to the free ligand values. Nevertheless, this shielding effect might be explained by the influence of the anisotropic effect of the neighbor phosphino aromatic rings. Table 3 compares the ^{1}H NMR chemical shifts of the free and coordinated 1-butylimidazole for the family [Ru(η^5-C_5H_5)(LL)(1-BuIm)][Z] (**1**–**6**) in $(CD_3)_2CO$.

^{13}C NMR spectra for this family of compounds confirm the evidence found for proton spectra. The Cp ring chemical shifts are in the range usually observed for Ru(II) cationic derivatives. All carbons of 1-butylimidazole ligand were only slightly deshielded or remained almost unchanged for the entire family of compounds.

^{31}P NMR spectra of the complexes showed a single sharp signal for the phosphine coligands revealing the equivalence of the two phosphorus atoms, and an expected deshielding upon coordination according to the σ donor character of these ligands. For compounds with the PPh_3 coligand this resonance occurred at ~42 ppm and for DPPE containing compounds this value was ~83 ppm. In compounds **2** and **5** was also found the characteristic septuplet signal of PF_6^- at −144.1 ppm.

Table 3
Selected ^{1}H NMR data for compounds [Ru(η^5-C_5H_5)(LL)(1-BuIm)][Z] (1–6) and the free ligand in $(CD_3)_2CO$.

Compound	Proton number							
	H1	H2	H3	H4	H5	H6	H7	Cp
1-BuIm	7.56	7.09	6.94	3.99	1.72	1.26	0.90	–
1	7.22	7.13	7.18	3.73	1.44	0.94	0.76	4.56
2	7.20	7.13[a]	7.13[a]	3.71	1.43	0.94	0.76	4.56
3	7.13[a]	7.07	7.22	3.67	1.42	0.93	0.76	4.55
4	6.57	6.34	6.62	3.40	1.19	0.91	0.76	4.75
5	6.53	6.36	6.63	3.39	1.19	0.90	0.76	4.75
6	6.50	6.35	6.60	3.37	1.18	0.89	0.76	4.74

[a] Overlap with PPh_3.

3.3. UV–visible studies

The optical absorption spectra of all the synthesized new complexes were recorded in ~5×10^{-5} mol dm^{-3} solutions of dichloromethane and are presented on Table 4.

The spectra of the compounds are essentially analogous to the ruthenium starting material complexes and are characterized by intense absorption bands in the UV region, at ~250 nm characteristic of π–π^* transitions of the aromatic ligands. This band was followed by one or two broad and less intense bands, which maximum is place between 300 and 400 nm. Fig. 1 is representative of the electronic spectra of this family of compounds.

Comparison of the electronic spectra of the studied compounds in solvents of different polarity, namely acetonitrile, acetone and dichloromethane revealed little effect of the solvent.

3.4. Electrochemical studies

The electrochemical behavior of the redox-active compounds **1**–**6** have been studied at room temperature by cyclic voltammetry

Table 4
Optical spectra data for complexes [Ru(η^5-C_5H_5)(LL)(1-BuIm)][Z] (1–6) and the free ligand, in dichloromethane, acetone and acetonitrile solutions.

Compound	λ_{max} (nm) (ε M^{-1} cm^{-1})		
	CH_2Cl_2	$(CH_3)_2CO$	CH_3CN
[Ru(η^5-C_5H_5)(PPh_3)$_2$(1-BuIm)]	233 (40,700)	–	205 (99,800)
[CF_3SO_3] (1)	–	–	–
	364 (2980)	367 (2290)	363 (2790)
[Ru(η^5-C_5H_5)(PPh_3)$_2$(1-BuIm)]	236 (21,600)	–	202 (9350)
[PF_6] (2)	291 (3670)	–	230 (sh)
	364 (2230)	363 (2240)	364 (2020)
[Ru(η^5-C_5H_5)(PPh_3)$_2$(1-BuIm)]	239 (38,000)	–	204 (11,900)
[BPh_4] (3)	271 (sh)	–	234 (sh)
	364 (3120)	363 (2300)	364 (2040)
[Ru(η^5-C_5H_5)(DPPE)(1-BuIm)]	234 (34,300)	–	203 (60,200)
[CF_3SO_3] (4)	291 (sh)	–	298 (sh)
	377 (1790)	381 (1850)	380 (1170)
[Ru(η^5-C_5H_5)(DPPE)(1-BuIm)]	236 (23,900)	–	201 (77,800)
[PF_6] (5)	290 (sh)	–	302 (sh)
	377 (1450)	381 (1322)	380 (1340)
[Ru(η^5-C_5H_5)(DPPE)(1-BuIm)]	248 (50,300)	–	211 (78,900)
[BPh_4] (6)	306 (sh)	–	316 (sh)
	385 (1990)	381 (1550)	382 (1630)

sh: shoulder.

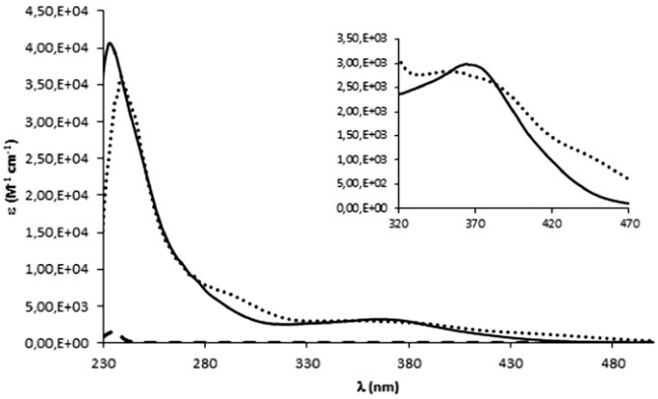

Fig. 1. Electronic spectra of $[Ru(\eta^5\text{-}C_5H_5)(PPh_3)_2(1\text{-BuIm})][CF_3SO_3]$ (1) (–), $[Ru(\eta^5\text{-}C_5H_5)(PPh_3)_2Cl]$ (•••••) and 1-BuIm ( ) in ~5 × 10^{-5} mol dm^{-3} dichloromethane solutions. Inset: detail of the charge transfer band.

(CV) at a platinum disk electrode in dichloromethane and acetonitrile with tetrabutylammonium hexafluorophosphate as supporting electrolyte. The results are summarized on Table 5 and typical CV's are showed on Fig. 2.

Upon scanning anodically, all the complexes (**1**–**6**) exhibit, in dichloromethane, one reversible oxidative response ($\Delta E = 80$ mV), in the potential range 0.90–1.05 V at the scan rate 200 mV s^{-1} assigned to the couple Ru^{II}/Ru^{III}. These results are within the range observed before for the related complexes $[Ru(\eta^5\text{-}C_5H_5)(PPh_3)_2(ImH)][PF_6]$

Table 5
Electrochemical data for complexes $[Ru(\eta^5\text{-}C_5H_5)(PP)(1\text{-BuIm})][Z]$ in dichloromethane and acetonitrile.

		E_{pa} (V)	E_{pc} (V)	$E_{1/2}$ (V)	$E_{pa}-E_{pc}$ (mV)	i_c/i_a
Dichloromethane						
1-BuIm		1.35	–	–	–	–
1	PP = $2PPh_3$	0.96	0.88	0.92	80	1.0
	Z = CF_3SO_3	1.58	–	–	–	–
2	PP = $2PPh_3$	0.56	0.48	0.52	80	0.9
	Z = PF_6	1.03	0.95	0.99	80	0.9
3	PP = $2PPh_3$	0.87	–	–	–	–
	Z = BPh_4	1.10	1.02	1.04	80	1.0
		1.49	–	–	–	–
4	PP = Dppe	0.94	0.86	0.90	80	0.95
	Z = CF_3SO_3	1.59	–	–	–	–
5	PP = Dppe	0.98	0.90	0.94	80	0.91
	Z = PF_6	1.64	–	–	–	–
6	PP = Dppe	0.85	0.76	–	90	0.4
	Z = BPh_4	1.49	–	–	–	–
Acetonitrile						
1-BuIm		1.48	–	–	–	–
		–	−0.66	–	–	–
		–	−1.55	–	–	–
1	PP = $2PPh_3$	0.98	–	–	–	–
	Z = CF_3SO_3	1.45	–	–	–	–
		–	−0.77	–	–	–
2	PP = $2PPh_3$	0.63	0.56	0.60	70	–
	Z = PF_6	1.01	–	–	–	–
		1.33	–	–	–	–
		–	−0.80	–	–	–
3	PP = $2PPh_3$	0.79	–	–	–	–
	Z = BPh_4	0.95[sh]	–	–	–	–
		1.22	–	–	–	–
		–	−0.13	–	–	–
		–	−0.75	–	–	–
4	PP = Dppe	0.81	0.74	0.78	70	0.95
	Z = CF_3SO_3					
5	PP = Dppe	0.82	0.75	0.79	70	1.0
	Z = PF_6					
6	PP = Dppe	0.90	0.70	–	200	0.43
	Z = BPh_4					

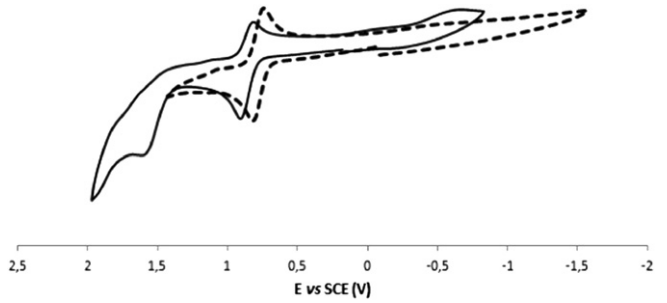

Fig. 2. Cyclic voltammogram of complex $[Ru(\eta^5\text{-}C_5H_5)(DPPE)(1\text{-BuIm})][PF_6]$ in dichloromethane (——) and acetonitrile (– – –) tipyfying the electrochemical behavior of these family of compounds.

Table 6
Selected bond lengths and bond and torsion angles for $[Ru(\eta^5\text{-}C_5H_5)(PPh_3)_2(1\text{-BuIm})][CF_3SO_3]$ 1, $[Ru(\eta^5\text{-}C_5H_5)(PPh_3)_2(1\text{-BuIm})][PF_6]$ 2, $[Ru(\eta^5\text{-}C_5H_5)(PPh_3)_2(1\text{-BuIm})][BPh_4]$ 3.

Compound	**1**		**2**	**3**	
	Molecule 1	Molecule 2		Molecule 1	Molecule 2
Bond lengths (Å)					
Ru–Cp[a]	1.846 (1)	1.853(1)	1.856 (3)	1.853(7)	1.856(7)
Ru–P(1)	2.370 (2)	2.338(2)	2.3472(7)	2.366(1)	2.319 (1)
Ru–P(2)	2.338 (2)	2.337 (2)	2.344 (1)	2.320(1)	2.349 (1)
Ru–N(1)	2.149(5)	2.131(6)	2.127(3)	2.126(3)	2.131(3)
Angles (°)					
Cp[a]–Ru–P(1)	121.74(5)	117.85(5)	119.22(2)	125.79(11)	122.26(8)
Cp[a]–Ru–P(2)	118.57(5)	123.85(5)	124.60(2)	120.43(7)	117.94(3)
Cp[a]–Ru–N(1)	121.04(14)	124.78(15)	124.17(6)	119.42(3)	125.05(11)
Ru–N(1)–C(11)	133.5(5)	125.3(5)	124.8(2)	125.9(3)	124.1(3)
Ru–N(1)–C(13)	121.8(5)	129.8(5)	130.0(2)	128.7(3)	130.8(3)
P(1)–Ru–P(2)	97.99(7)	102.31(7)	100.60(3)	106.24(3)	104.55(3)
N(1)–Ru–P(1)	95.20(16)	92.75(16(	91.76(6)	90.50(9)	87.85(9)
N(1)–Ru–P(2)	96.70(16)	87.78(16)	88.26(7)	87.07(8)	92.07(9)

[a] Centroid of the η^5-cyclopentadienyl ligand.

($E_{1/2}$ = 1.04 V) and $[Ru(\eta^5\text{-}C_5H_5)(PPh_3)_2(1\text{-BI})][CF_3SO_3]$ ($E_{1/2}$ = 0.90 V)in the same experimental conditions [12,13] indicating that the chemically linked alkyl pendent arm have a negligible contribution on the ruthenium(II) oxidation process. In addition, another redox process was also found ~1.5 V for all the studied compounds attributed to the oxidation at imidazole coordinated molecule. Unexplainably, another oxidation process, at a much lower potential, was found for complexes **2** and **3** which was postulated to occur in the 1-butylimidazole coordinated ligand and may possibly

Table 7
Selected bond lengths and bond and torsion angles for $[Ru(\eta^5\text{-}C_5H_5)(DPPE)(1\text{-BuIm})][CF_3SO_3]$ 4, $[Ru(\eta^5\text{-}C_5H_5)(DPPE)(1\text{-BuIm})][PF_6]$ 5, $[Ru(\eta^5\text{-}C_5H_5)(DPPE)(1\text{-BuIm})][BPh_4]$ 6.

Compound	**4**	**5**	**6**
Bond lengths (Å)			
Ru–Cp[a]	1.863 (1)	1.861 (1)	1.860(1)
Ru–P(1)	2.275(1)	2.278(1)	2.269(1)
Ru–P(2)	2.283 (1)	2.286 (1)	2.289(1)
Ru–N(1)	2.131(2)	2.141(3)	2.133(2)
Angles (°)			
Cp[a]–Ru–P(1)	128.65(2)	123.37(8)	124.80(2)
Cp[a]–Ru–P(2)	126.04(2)	127.54(3)	127.05(2)
Cp[a]–Ru–N(1)	123.59(6)	127.09(3)	122.68(7)
Ru–N(1)–C(11)	130.49(17)	130.7(3)	124.9(2)
Ru–N(1)–C(13)	124.97(17)	124.2(3)	130.0(2)
P(1)–Ru–P(2)	84.04(3)	84.04(3)	84.50(3)
N(1)–Ru–P(1)	88.23(6)	89.41(8)	92.39(7)
N(1)–Ru–P(2)	94.28(6)	93.43(9)	94.70(7)

[a] Centroid of the η^5-cyclopentadienyl ligand.

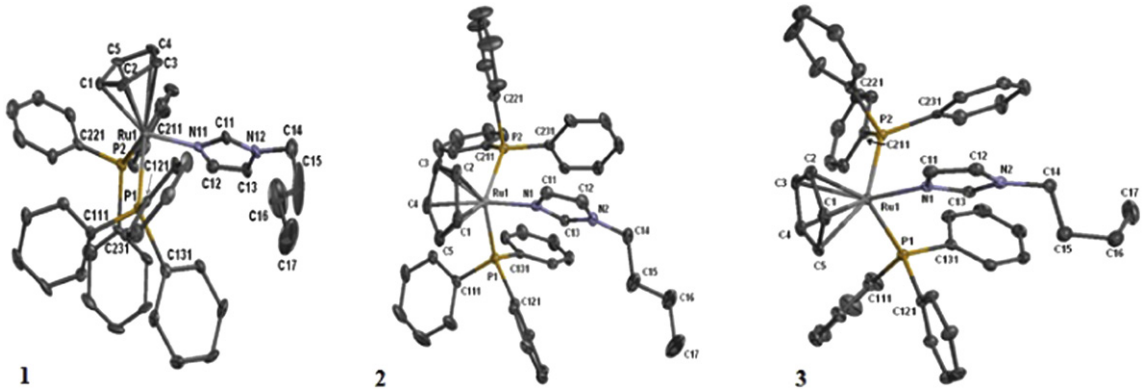

Fig. 3. Molecular diagrams depicting the cationic moieties for complexes 1–3. Hydrogen atoms were omitted for clarity. The different conformation of the aliphatic side chain of the 1-butylimidazole can be clearly observed. For compounds 1 and 3 only one molecule is depicted.

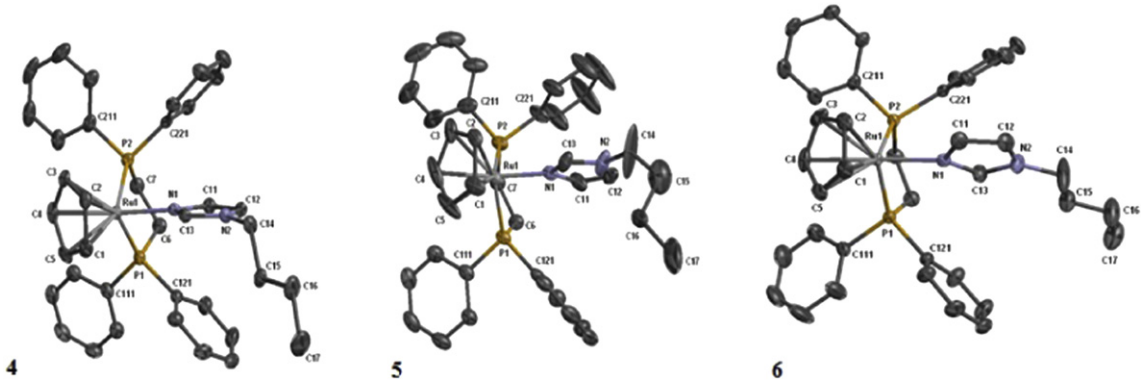

Fig. 4. Molecular diagrams depicting the cationic moieties for complexes 4–6. Hydrogen atoms were omitted for clarity. The different conformation of the aliphatic side chain of the 1-butylimidazole is again clearly evidenced.

reflect some modification of the electronic features of the 1-BuIm ligand through metal complexation. In effect, complex **2** (with PF_6 as counter ion), showed a quasi reversible oxidation at $E_{1/2} = 0.52$ V, while this process was irreversible for complex **3** (with BPh_4 as counter ion) with an anodic wave at $E_{pa} = 0.87$ V. The cyclic voltammograms obtained in acetonitrile for complexes **1**–**3** were characterized, at positive potentials, by the Ru^{II}/Ru^{III} irreversible process in the range 0.95–1.01 V. As observed in dichloromethane, also the process occurring at lower potentials attributed to the coordinated imidazole was found quasi reversible for complex **2** ($E_{1/2} = 0.60$ V) and irreversible for complex **3** ($E_{pa} = 0.79$).

The anodic scan gives for complexes **4** and **5**, a reversible Ru^{II}/Ru^{III} redox wave at 0.81 and 0.82 V, respectively. The similarity of these oxidation potentials indicates the negligible contribution of the non-coordinating anions PF_6^- and $CF_3SO_3^-$ on the ruthenium redox potentials. Ratios of reverse to forward currents (i_c/i_a) of 1.0 and 0.95 V at a scan rate of 200 mV s^{-1} presented by complexes **4** and **5**, showed that the oxidized forms display high chemical stability on the time scale of the cyclic voltammetry experiment. The lower stability of compound **6** presenting the BPh_4^- as counter ion ($E_{pa} = 0.90$ V), with the value of i_c/i_a ratio of 0.4 is in agreement with the result also found in dichloromethane.

Our electrochemical studies reveal that the DPPE derivatives present redox potentials for the Ru^{II}/Ru^{III} couple slightly lower than those of the correspondent triphenylphosphine analogs, particularly in acetonitrile. This can be expected on the basis of the greater electro-withdrawing power of triphenylphosphine in comparison

Fig. 5. Superimposition of the cationic fragments of $CpRu(1\text{-BuIm})(PPh_3)_2$. Phenyl rings and H atoms have been omitted for clarity. Perfectly evidenced is the different geometries adopted by the N-heterocyclic rings and the butyl chains. (dark blue: molecule 1 of 1; red: molecule 2 of 1; pale blue: compound **2**; green: molecule 1 of 3 and magenta: molecule 2 of 3). (For interpretation of the references to color in this figure legend, the reader is referred to the web version of this article.)

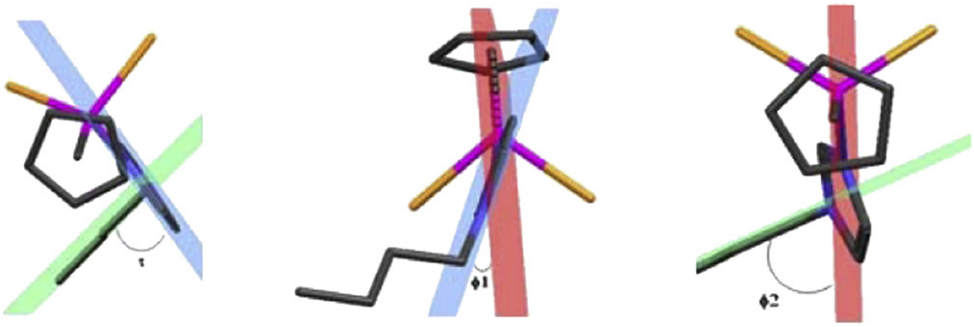

Scheme 2. Definition of the angles φ_1, φ_2 and τ : for details see text above.

with the bidentate DPPE and the reduced π-backdonation ability of the ruthenium center.

3.5. X-ray structural studies of complexes

In this family of ruthenium complexes bearing a 1-butylimidazole ligand, we are looking for the influence of the mono and bidentate phosphine ligand in the overall coordination geometry of the Ru core. The effect of the counter ion not only in the geometry but also in the overall packing, governing the behavior of the newly synthesized compounds is also studied here.

Suitable crystals for X-ray diffraction studies of the complexes with triphenylphosphine ligands (**1**–**3**), crystallized in different crystalline systems and space groups (monoclinic, $P2_1/c$ for **1**, triclinic, P-1 for **2** and orthorhombic P c a 2_1 for **3**). Complexes with DPPE (**4**–**6**) all crystallized in the same crystalline systems and space group monoclinic, $P2_1/n$.

All compounds present the usual distorted three-legged piano stool geometry for η^5-monocyclopentadienyl complexes confirmed by P–M–P angles of 97.99(7)° to 106.24(3) and N–M–P angles varying from 87.07(8)° to 96.70(16), with the remaining η^5-Cp(centroid)–M–X (with X = N or P) angles between 117.85(5)° and 125.05(11)° for complexes **1**–**3** (see Table 6). In complexes **4**–**6** the geometry is restricted by the stereochemical imposition of the bite angle of the bidentate phosphine, with P–M–P angles below 90°, 84.04(3) to 84.50(3) and N–M–P angles varying from 88.23(6)° to 94.70(7), with the remaining η^5-Cp(centroid)–M–X (with X = N or P) angles between 122.68(7)° and 128.65(2)° (see Table 7).

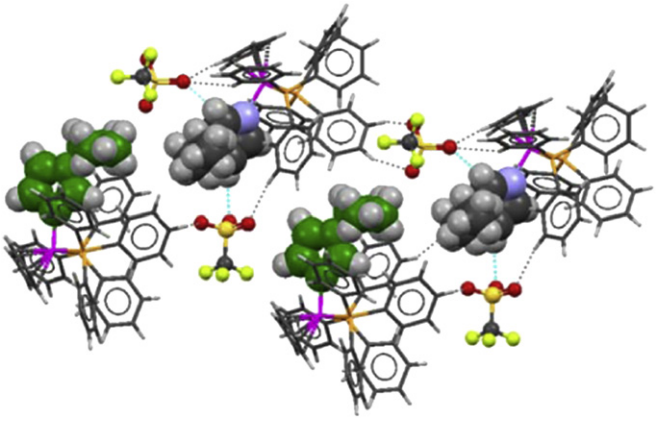

Fig. 6. Supramolecular packing showing the intermolecular hydrogen bonds of the butylimidazole ligand to the counter ion. (Bulm fragment of molecule 2 is green and gray: turquoise: intermolecular interactions described in the text). (For interpretation of the references to color in this figure legend, the reader is referred to the web version of this article.)

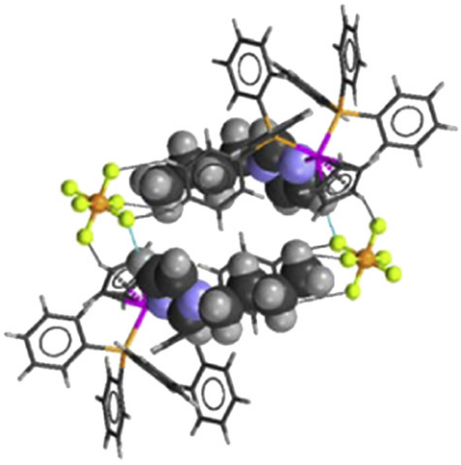

Fig. 7. Supramolecular packing showing the intermolecular hydrogen bonds of the butylimidazole ligand to the counter ion. (turquoise: intermolecular interactions described in the text). (For interpretation of the references to color in this figure legend, the reader is referred to the web version of this article.)

The distances Ru-η^5-Cp(centroid), ranging from 1.846(1) to 1.863(2) Å, and Ru–N ranging from 2.126(3) and 2.149(5) Å are well within the values expected for this family of compounds [36]. Also expected are the slightly longer Ru–P distances in compounds

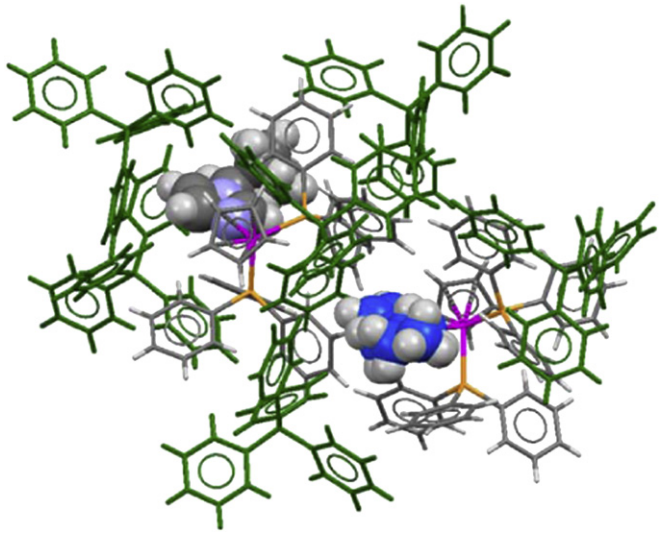

Fig. 8. Supramolecular packing showing the structural involvement of the 1-Bulm fragment in the two different molecules.

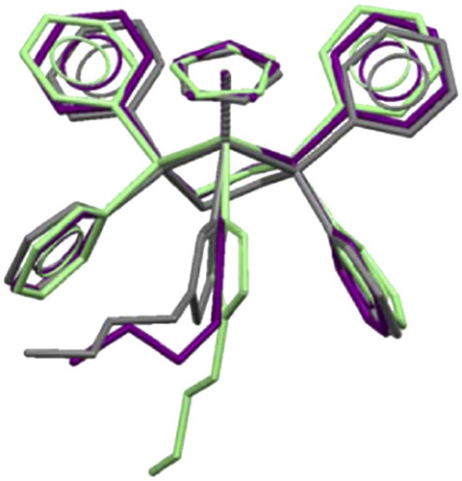

Fig. 9. Superimposition of the cationic fragments of CpRu(1-BuIm)(DPPE). H atoms have been omitted for clarity. Phenyl rings are represented to show the restrictions imposed. Geometries adopted by the N-heterocyclic rings and the butyl chains are shown. (gray: compound 4; purple: compound 5; green: compound 6). (For interpretation of the references to color in this figure legend, the reader is referred to the web version of this article.)

1–**3** when compared with the ones in **1**–**4**, respectively 2.319(1)–2.370(2) Å versus 2.269(1) and 2.289(1) Å [11,23,37].

In Fig. 3 we present the ORTEP molecular diagrams of compounds **1**–**3** and in Fig. 4 the corresponding ones for **4**–**6**, for sake of comparison the same labeling is used in the 1-butylimidazole ligand.

While the overall coordination geometry of the cations is similar and comparable to other η^5, η^6 aryl Ru complexes [11,24,38], the geometry of the 1-butylimidazole ligand is considerably different in all six compounds. The occurrence of different conformations within imidazole derivatives was already noticed in previous studies of Ru derivatives with η^6 arene with imidazole ligands, and as expected the longer the chain the higher is the distortion [25,39].

Comparing the conformation of the 1-butylimidazole (1-BuIm) within the $CpRu(PPh_3)_2$ complexes we can see in Fig. 5, that they are very different. To better characterize the geometry and distortion of the fragment we have defined the angles φ_1, φ_2 and τ : φ_1 is the dihedral angle between the plane containing Ru, η^5-Cp(centroid), and the coordinated N atom of the imidazole ring and the ring plane of the heterocycle; φ_2 is the angle between the first plane and the plane containing the four carbon atoms of the butyl chain; τ is the angle, between the N-heterocycle ring and the plane of the butyl chain, defining the geometry within the ligand. These angles are illustrated in Scheme 2 (Fig. 6).

In complex **1** there are two molecules in the asymmetric unit and the two of them have completely different conformations, with $\varphi_1 = 53.8^\circ$, $\varphi_2 = 66.0^\circ$ and $\tau = 60.9^\circ$ for molecule 1 and $\varphi_1 = 21.5^\circ$, $\varphi_2 = 83.8^\circ$ and $\tau = 82.5^\circ$ for molecule 2. Observing the neighborhood of the two fragments we can see that in molecule 1 the 1-BuIm interacts with two CF_3SO_3 anions through $CH_{buim\ ring}\cdots O_{anion}$ (2.47 and 2.60 Å) while in molecule 2 the fragment is isolated. This can explain the different geometries of the fragment in the two molecules of compound **1**.

In compound **2** the 1-BuIm conformation is defined by $\varphi_1 = 23.9^\circ$, $\varphi_2 = 65.5^\circ$ and $\tau = 83.2^\circ$ and we can see that there is an interaction of the type $CH_{buim\ ring}\cdots F_{anion}$ of 2.56 Å, the aliphatic chain having no shorter intermolecular interactions. (Fig. 7)

In compound **3** the different conformation of the 1-BuIm ligand, $\varphi_1 = 20.5^\circ$, $\varphi_2 = 81.5^\circ$ and $\tau = 88.3^\circ$ for molecule 1 and $\varphi_1 = 14.4^\circ$, $\varphi_2 = 52.7^\circ$ and $\tau = 42.0^\circ$ for molecule 2, is mainly due to stereochemical hindrance imposed by the bulkiness of the anion and has a more pronounced effect on φ_2 and τ, assessing the relative positioning of the alkyl chain. (Fig. 8)

As can be seen the supramolecular arrangement, stereochemical hindrance and intermolecular interactions are determinant in the final conformation of the ligand.

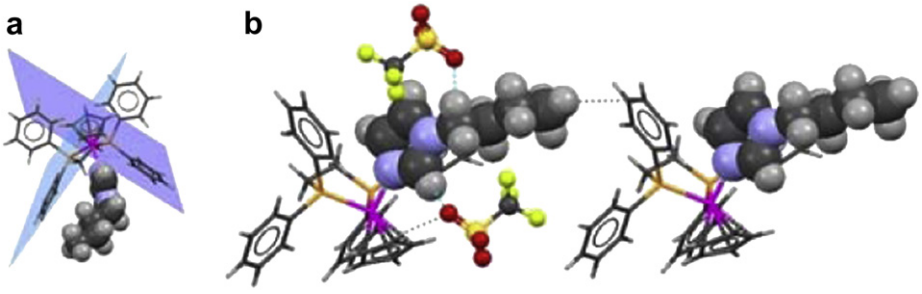

Fig. 10. a) Inset showing the stereochemical imposition of the phenyl rings b) Supramolecular packing showing the intermolecular hydrogen bonds of the butylimidazole ligand to the CF_3SO_3 counter ion.

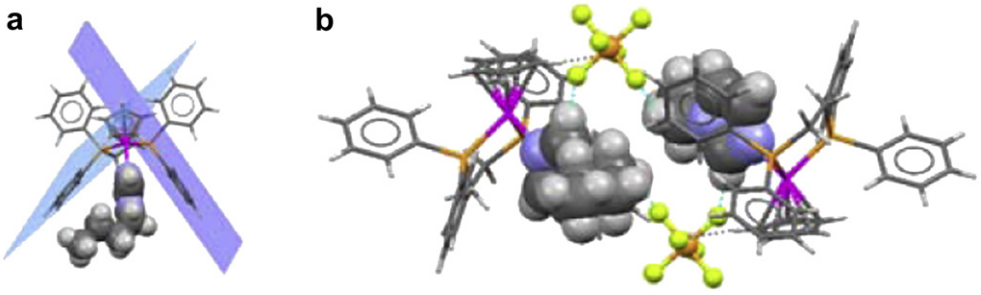

Fig. 11. a) Inset showing the stereochemical imposition of the phenyl rings b) Supramolecular packing showing the intermolecular hydrogen bonds of the butylimidazole ligand to the PF_6 anion.

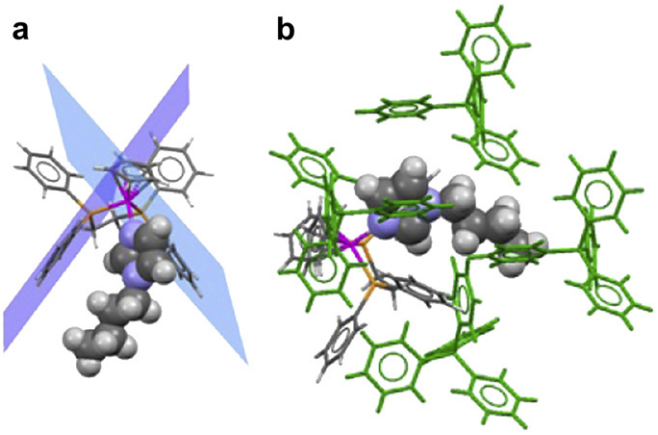

Fig. 12. a) Inset showing the stereochemical imposition of the phenyl rings b) Supramolecular packing showing the intermolecular hydrogen bonds of the butylimidazole ligand to the PF_6 anion.

Analyzing the compounds bearing the DPPE ligand we can see that the conformation of the ligand is more restricted due to the stereochemistry of the DPPE fragment, with the phenyl rings reducing the possible geometries adopted by the 1-BuIm, with the φ_1 angle showing a less significant variation than previously, 5.0°, 3.8° and 20.6°, in compounds **4** to **6** respectively.

In compounds **4** and **5**, due to the small values of φ_1, the two remaining angles are very similar, as expected ($\varphi_2 = 86.6°$ and $\tau = 87.0°$ for **4** and $\varphi_2 = 74.8°$ and $\tau = 78.6°$ for **5**), showing that the tilting of the N-heterocyclic ring is restricted but that the relative positioning of the aliphatic chain is due to its intermolecular interactions. In **4** there is one short $CH_{buim\ ring}\cdots O_{anion}$ of 2.52 Å and also a $CH_{buim\ chain}\cdots O_{anion}$ of 2.66 Å, governing the torsion of the molecule. In **5** the same type of interaction with the counter ion is noticed and the same carbon atoms from both the ring and alkyl moiety of buim are involved, atoms C13 and C14, with distances of $CH_{buim\ ring}\cdots F_{anion}$ of 2.38 Å and also a $CH_{buim\ chain}\cdots F_{anion}$ of 2.52 Å. Figs. 9 and 10 show the supramolecular arrangements (Fig. 11).

Compound **6** is shown to have a particular conformation, different from all the others, $\varphi_1 = 20.6$, $\varphi_2 = 25.7°$ and $\tau = 5.6°$ due to the "phenylic surrounding" of the fragment imposing strong stereochemical restrictions. (Fig. 12)

4. Conclusions

We here have described the synthesis of new ruthenium(II) organometallic complexes with the formula $[Ru(\eta^5\text{-}C_5H_5)(LL)(1\text{-BuIm})]$ [Z], with (LL) = $2PPh_3$ or DPPE, and Z = $CF_3SO_3^-$, PF_6^-, BPh_4^-, with coordinated 1-butylimidazole. ^1H NMR spectroscopic data revealed the electron-donor effect of the organometallic fragments $\{RuCp(L{-}L)\}^+$ to the ring of the coordinated 1-butylimidazole through an effect of π-backdonation. This effect was also extended to the pendent arm, as revealed by the significant values of shielding of these protons. The magnitude of this effect is more evident for the compounds with DPPE as coligand than with $2PPh_3$, this showing the different contribution of these two coligands for the electronic properties of the $\{RuCp(L{-}L)\}^+$ fragment. The influence of these mono and bidentate phosphanes was also evidenced by means of X-ray structural studies, which revealed that the presence of these two coligands definitely influences the occurrence of different conformations for the 1-butylimidazole coordinated ligand, within this family of compounds. Moreover, the presence of DPPE or $2PPh_3$ clearly controls the interaction of 1-butylimidazole with the counter ion. As a result of this important interaction compound **2** could reversibly be oxidized at the coordinated 1-butylimidazole.

The major interest of the present study, besides the enlargement of the family of the general formula $[Ru(\eta^5\text{-}C_5H_5)(LL)(L')][Z]$ that revealed already potential cytotoxic properties against tumor cells, is the finding that the electronic properties of the effective ligand (L′) can significantly be influenced by the coligands (LL) and the couter ions (Z). Thus, important interaction with serum proteins and/or DNA are envisaged to occur preferentially for compounds with PPh_3 namely the series $[Ru(\eta^5\text{-}C_5H_5)(PPh_3)_2(1\text{-BuIm})][Z]$.

Acknowledgments

We thank to Fundação para a Ciência e Tecnologia for financial support (PTDC/QUI/66148/2006 and REDE/1501/REM/2005). Tânia S. Morais thanks FCT for her Ph.D Grant (SFRH/BD/45871/2008).

Appendix A. Supplementary material

Crystallographic data for the structural analysis of compounds **1**–**6** was deposited at the Cambridge Crystallographic Data Centre under the numbers CCDC 865875–865880. These data can be obtained free of charge via www.ccdc.cam.ac.uk or from the Cambridge Crystallographic Data Centre, 12 Union Road, Cambridge CB21EZ, U.K., e-mail deposit@ccdc.cam.ac.uk.

References

[1] J.M. Rademaker-Lakhai, D. van den Bongard, D. Pluim, J.H. Beijnen, J.H.M. Schellens, Clin. Cancer Res. 10 (2004) 3717.
[2] C.G. Hartinger, S. Zorbas-Seifried, M.A. Jakupec, B. Kynast, H. Zorbas, B.K. Keppler, J. Inorg. Biochem. 100 (2006) 891.
[3] W.H. Ang, P.J. Dyson, Eur. J. Inorg. Chem. (2006) 2003.
[4] P.J. Dyson, Chimia 61 (2007) 698.
[5] W.J. Zeller, S. Fruhauf, G. Chen, B.K. Keppler, E. Frei, M. Kaufmann, Eur. J. Cancer 27 (1991) 62.
[6] M. Coluccia, G. Sava, F. Loseto, A. Nassi, A. Boccarelli, D. Giordano, E. Alessio, G. Mestroni, Eur. J. Cancer 29A (1993) 1873.
[7] M.J. Clarke, Coord. Chem. Rev. 236 (2003) 209.
[8] E. Alessio, G. Mestroni, A. Bergamo, G. Sava, in: A. Sigel, H. Sigel (Eds.), Metal Ions in Biological Systems. Metal Complexes in Tumor Diagnosis and as Anticancer Agents, vol. 42, Marcel Dekker, New York, 2004, pp. 323–351.
[9] Y.K. Yan, M. Melchart, A. Habtermariam, P.J. Sadler, Chem. Comm. 38 (2005) 4764.
[10] S.J. Dougan, P.J. Sadler, Chimia 61 (2007) 704.
[11] M.H. Garcia, T.S. Morais, P. Florindo, M.F.M. Piedade, V. Moreno, C. Ciudad, V. Noe, J. Inorg. Biochem. 103 (2009) 354.
[12] V. Moreno, J. Lorenzo, F.X. Aviles, M.H. Garcia, J. Ribeiro, T.S. Morais, P. Florindo, M.P. Robalo, Bioinorg. Chem. Appl. (2010).
[13] V. Moreno, M. Font-Bardia, T. Calvet, J. Lorenzo, M.H. Garcia, T.S. Morais, A. Valente, M.P. Robalo, J. Inorg. Biochem. 105 (2011) 24.
[14] B. Fromenty, D. Pessayre, Pharmacol. Ther. 67 (1995) 101.
[15] R.K. Kutty, G. Santostasi, J. Horng, G. Krishna, Toxicol. Appl. Pharmacol. 107 (1991) 377.
[16] R.E. Heikkila, J. Hwang, S. Ofori, H.M. Geller, W.J. Nicklas, J. Neurochem. 54 (1990) 743.
[17] T. Aiuchi, Y. Shirane, H. Kinemochi, Y. Arai, K. Nakaya, Y. Nahamura, Neurochem. Int. 12 (1988) 525.
[18] L.M. Sayre, F. Wang, C.L. Hoppel, Biochem. Biophys. Res. Commun. 161 (1989) 809.
[19] R.R. Rqamsay, R.J. Mehlhom, T.P. Singer, Biochem. Biophys. Res. Commun. 159 (1989) 983.
[20] A. Berson, V. De Beco, P. Letteron, M.A. Robin, C. Moreau, J. El Kahwaji, N. Verthier, G. Feldmann, B. Fromenty, D. Pessayre, Gastroenterology 114 (1998) 764.
[21] A. Berson, V. Descatoire, A. Sutton, D. Fau, B. Maulny, N. Vadrot, G. Feldmann, B. Berthon, T. Tordimann, D. Pessayre, Pharmacol. Ther. 299 (2001) 793.
[22] B.T. Loughrey, P.C. Healy, P.G. Parsons, M.L. Williams, Inorg. Chem. 47 (2008) 8589.
[23] M.H. Garcia, T.S. Morais, A.I. Tomaz, F.M. Marques, F. Mendes, "Transition metal complexes for pharmaceutical applications", Patent application PT105890;
[24] D.D. Perrin, W.L.F. Armarego, D.R. Perrin, in: Purification of Laboratory Chemicals, second ed. Pergamon, New York, 1980.
[25] M.I. Bruce, N.J. Windsor, Aust. J. Chem. 30 (1977) 1601.
[26] G.S. Ashby, M.I. Bruce, I.B. Tomkins, R.C. Walli, Aust. J. Chem. 32 (1979) 1003.
[27] N.G. Conelly, W.E. Geiger, Chem. Rev. 96 (1996) 877.
[28] SABADS, Area-detector Absorption Correction, Brucker AXS Inc., Madinson, WI, 2004.

[29] SAINT, Area-detector Integration Software (Version 7.23), Brucker AXS Inc., Madinson, WI, 2004.
[30] A. Altomare, M.C. Burla, M. Camalli, G. Cascarano, G. Giacovazzo, A. Guagliardi, A.G.G. Moliterini, G. Polidoro, R. Spagna, J. Appl. Cryst. 32 (1999) 115.
[31] G.M. Sheldrick, Acta Cryst. A64 (2008) 112.
[32] G.M. Sheldrick, SHELXL-97: Program for the Refinement of Crystal Structure, University of Gottingen, Germany, 1997.
[33] L.J. Farrugia, J. Appl. Cryst. 32 (1999) 837.
[34] L.J. Farrugia, J. Appl. Cryst. 30 (1997) 565.
[35] C.F. Macrae, P.R. Edgington, P. McCabe, E. Pidcock, G.P. Shields, R. Taylor, M. Towler, J. Van de Streek, J. Appl. Cryst. 39 (2006) 453.
[36] F.H. Allen, Acta Cryst. B58 (2002) 380.
[37] M.H. Garcia, P. Florindo, M.F.M. Piedade, M.T. Duarte, M.P. Robalo, E. Goovaerts, W. Wemseleers, J. Organomet. Chem. 694 (3) (2009) 433.
[38] C.A. Vock, C. Scolaro, A.D. Phillips, R. Scopelliti, G. Sava, P.J. Dyson, J. Med. Chem. 49 (2006) 5552.
[39] M. Groessl, E. Reisner, C.G. Hartinger, R. Eichinger, O. Semenova, A.R. Timerbaev, M.A. Jakupec, V.B. Arion, B.K. Keppler, J. Med. Chem. 50 (2007) 2185.